

Crack Damage Propagation and Morphology Distribution of Hydraulic Electric Pulse Fractured Coal

Xiankai Bao, Wu Zhang,* Shuang Zhao, Ning Wu, Chaoyun Yu, Jinchang Zhao, and Wenxiang Zheng



Cite This: *ACS Omega* 2023, 8, 16032–16046

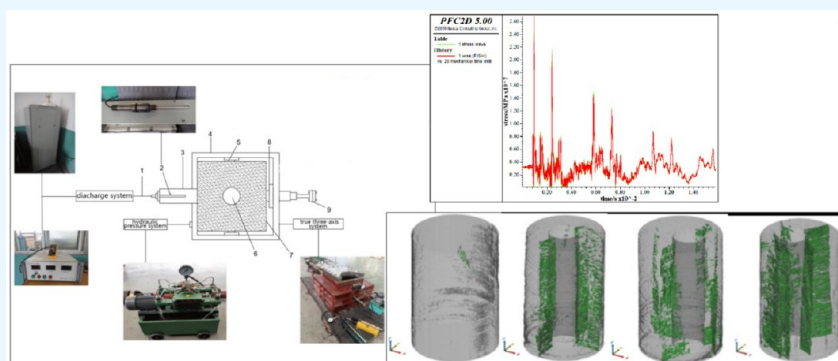


Read Online

ACCESS |

Metrics & More

Article Recommendations



ABSTRACT: This work discusses the damage and failure effect of a hydraulic electric pulse and the law of crack growth on coal. The impact and failure effect of a water shock wave and the mechanism of crack initiation, propagation, and arrest were studied by numerical simulation and the fracturing test of coal, combined with CT scanning, PCAS software, and Mimics 3D reconstruction technology. The results show that a high voltage electric pulse that increases permeability is an effective artificial crack making technology. The crack spreads radially along the borehole, and the damage degree, number, and complexity were positively correlated with the discharge voltage and discharge times. The crack area, volume, damage factor, and other parameters increased steadily. The cracks in the coal first start from two symmetrical angles, and finally distribute in a 360 deg circumferential direction, forming a multiangle crack spatial network structure. The fractal dimension of the crack group increases, the number of microcracks and the roughness of the crack group increases, the overall fractal dimension of the specimen decreases, and the roughness between cracks weakens. The cracks then form a smooth coal-bed methane migration channel. The research results can provide some theoretical guidance for the evaluation of crack damage propagation and the effect of electric pulse fracturing in water.

1. INTRODUCTION

With the putting forward of the national green development strategy, energy saving, emission reduction, pollutant control, and dealing with climate change have become core development goals and strategies in China. China has abundant reserves of coal-bed methane (coal gas), and increasing the exploitation and utilization of coal-bed methane can not only alleviate the shortage of resources, but also achieve the purpose of preventing coal-bed methane outburst and protecting the environment. China's coal-bed methane has the characteristics of low permeability, low extraction efficiency, and low output. To improve the extraction efficiency of coal-bed methane, artificial crack manufacturing technology is an effective method. Static blasting technology,¹ hydraulic fracturing technology,² hydraulic slit technology,³ high voltage electric pulse increasing permeability technology^{4,5} have all greatly promoted the development of artificial crack manufacturing technology. High voltage electric pulse increasing permeability technology

has been widely used in the field of oil stimulation and plugging removal.

In 1955, Yutkin⁶ found that a high voltage discharge in liquid could produce huge mechanical effects. Since then, this physical phenomenon has been transformed into an engineering and technical problem of common concern in many fields. Buogo⁷ and Timoshkin⁸ analyzed the hydrodynamic process of bubbles in liquid, the energy flow in the growth process of bubbles, and the transport process of mass flow in the discharge process. Pingping Rao⁹ established a rock breaking model of electrical pulse, and proposed an analytical method to predict the

Received: December 25, 2022

Accepted: March 27, 2023

Published: April 21, 2023



mechanical behavior of high voltage electrical pulse by taking granite as an example. Xiankai Bao¹⁰ conducted fracturing tests with different water pressures and discharge voltages on coal samples, and studied the mechanism of crack initiation, damage characteristics, and propagation law of coal. Although the hydraulic electric effect has been studied in detail and successfully applied in the field of oil stimulation, it is still in the initial stage of theoretical research, and toward application in the field of improving the extraction conditions and extraction efficiency of unconventional natural gas, many problems still need to be studied and solved.

Compared with traditional fracturing methods, high voltage electric pulse increasing permeability technology not only has the advantages of environmental protection, water saving, and rapid repeated discharge, but also has the characteristics of good fracturing effect, fracture connectivity, and complex fracture network.^{11,12} However, it is hard to evaluate the fracturing effect because of the invisibility of the internal cracks in coal. Bao Xiankai¹³ conducted high-voltage electric pulse hydraulic fracturing tests on coal samples under the conditions of the same water pressure and different discharge voltages, and qualitatively analyzed the initiation, development, and distribution of internal cracks in coal samples from a two-dimensional perspective. Yin Zhiqiang¹⁴ studied the hydraulic and electrical characteristics of high voltage pulse discharge in water from the theoretical and experimental perspectives and evaluated the cracking effect of coal rock mass. Then Bao Xiankai^{15–17} used ultrasonic detection technology combined with a variety of advanced numerical simulation software to study the number and CT images to identify and extract cracks in coal core specimens. The parameters such as length, quantity, density, fracture rate, and fractal dimension are further used to quantitatively describe cracks. Although many scholars carried out extensive research work of high voltage electric pulse increasing permeability technology evaluation, due to the difficulties of direct observation of internal cracks and the heterogeneity of coal itself, the regularity of crack propagation under a water shock wave load of two-dimensional and three-dimensional space forms still needs further study. With the use of three-dimensional reconstruction technology to study the damage of rock mass and the with the increase of the internal pore fracture structure expansion law, scientific research gradually steps from the two-dimensional plane into three-dimensional space. Zhang Jieying¹⁸ developed a three-dimensional visualized rock mesoscopic damage evolution system and conducted in-depth research and analysis on the internal mesoscopic damage evolution process of oil shale under different temperatures and of mudstone under external load. Zhao Jing¹⁹ used a three-dimensional attenuation coefficient reconstruction technology to study the number, scale, and evolution characteristics of internal pores and fractures in oil shale. Some other experts and scholars have achieved qualitative or quantitative description of the internal pore and fracture structure of rock mass by using various software programs such as VGStudio MAX, Avizo, Mimics, Matlab, and corresponding advanced mathematical algorithms.^{20–24} Therefore, to accurately evaluate the effect of high voltage electric pulse hydraulic fracturing of coal, describe the spatial distribution morphology of cracks in coal specimens and study the propagation law, not only to evaluate and analyze the two-dimensional CT image, but also to study the spatial distribution of cracks in coal rock mass, the help of three-dimensional reconstruction technology is necessary.

In this paper, based on the classical theory of elastic-plastic mechanics and rock mechanics, the physical test and numerical simulation of coal under the same water pressure, different discharge voltages, and simulated in situ stress conditions are carried out to study the damage cracks, the initiation and propagation mechanism of cracks in coal, and the distribution pattern of cracks. Two-dimensional CT and three-dimensional reconstruction technology were used to visualize the internal cracks of coal after cracking. PCAS software and Mimics 3D reconstruction software were used to comprehensively analyze the two-dimensional and three-dimensional distribution characteristics of cracks in coal. Damage variables, rose plots, and fractal dimensions were used to evaluate the development, evolution, morphology distribution, and damage characteristics of cracks.

2. MECHANISM ANALYSIS AND NUMERICAL SIMULATION OF HIGH VOLTAGE ELECTRIC PULSE HYDRAULIC FRACTURING OF COAL

2.1. Mechanism Analysis of Crack Propagation in Coal.

Similar to what is formed in underwater blasting, coal will form a failure zone, plastic zone, and elastic zone under a hydraulic electric pulse load (Figure 1). After the high voltage discharge,

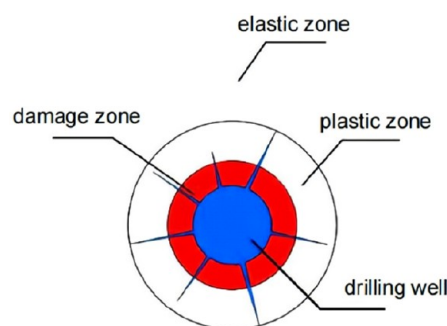


Figure 1. Regional distribution of coal under hydraulic and electric pulse load.

the water shock waves impact the coal at a high speed, resulting in the circumferential tensile stress. When the circumferential tensile stress near the borehole is greater than the dynamic tensile strength of coal, damage and cracks in coal occur. At the position where the crack has been generated, water will rush into the notch rapidly, leading to the stress concentration phenomenon at the crack tip and forming the water wedge effect and further propagation of the crack (Figure 2). The circumferential tensile stress generated by the water shock wave near coal drilling is²⁵

$$\sigma_{\theta} = P \frac{r^2}{r_0^2} - \left[\frac{\sigma_x + \sigma_y}{2} \left(1 + \frac{r^2}{r_0^2} \right) - \frac{\sigma_x - \sigma_y}{2} \left(1 + 3 \frac{r^2}{r_0^2} \right) \cos 2\theta - \tau_{xy} \left(1 + 3 \frac{r^2}{r_0^2} \right) \sin 2\theta \right] \quad (1)$$

where σ_{θ} is the circumferential stress, MPa; r is the linear distance from the axis of the borehole to any point of coal, m; r_0 is the radius of the borehole, m; σ_x , σ_y , and τ_{xy} are the in situ stress and shear stress components of horizontal x axis and vertical y axis, respectively, MPa; θ is the polar angle in the

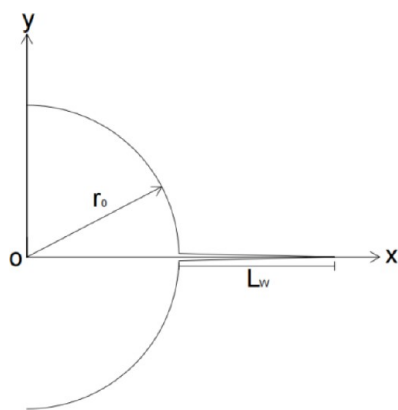


Figure 2. Schematic diagram of crack propagation with water wedge effect.

cylindrical coordinate system; P is the peak pressure of the first pressure pulse wave, MPa; which is taken as follows:

$$P = P_{\max} \quad (2)$$

The dynamic tensile strength of coal changes with the change of loading rate of dynamic load. The fitting regression formula is²⁶

$$\sigma_d = 0.244V^{0.430} \quad (3)$$

where σ_d is the dynamic tensile strength of coal, MPa. V is the loading rate, GPa/s,

$$V = \frac{P - P_w}{\tau} \quad (4)$$

where P is the actual stress of the water shock wave acting on the borehole wall, τ is the pressure wavefront time, s, which is 1.25 times the time interval between 10% peak time and 90% peak time of the water shock rising front; P_w is the water pressure value, MPa. Substituting eq 2 into eq 1 and eq 4 into eq 3:

$$\sigma_\theta = P_{\max} \frac{r^2}{r_0^2} - \left[\frac{\sigma_x + \sigma_y}{2} \left(1 + \frac{r^2}{r_0^2} \right) - \frac{\sigma_x - \sigma_y}{2} \left(1 + 3\frac{r^2}{r_0^2} \right) \cos 2\theta - \tau_{xy} \left(1 + 3\frac{r^2}{r_0^2} \right) \sin 2\theta \right] \quad (5)$$

$$\sigma_d = 0.244 \left(\frac{P_{\max} - P_w}{\tau} \right)^{0.430} \quad (6)$$

The compressive strength of coal is much greater than the tensile strength, the surface of the borehole takes the lead to meet the tensile strength first under the action of shock waves. Considering the influence of the gas pressure inside the coal, when $\sigma'_\theta = \sigma_\theta - p_2 \geq \sigma_d$ (where σ'_θ is the effective circumferential stress, p_2 is the gas pressure in the coal), and the coal will be damaged and cracks will start.

After crack initiation in coal, the crack continues to expand under the action of water wedge. Water wedge splitting is a physical phenomenon, tension-water wedge fracture is caused by the combined stress of shear, tension, and pressure on the rock mass,²⁷ leading to the crack extension. To study the water wedge effect, a crack is taken for research (Figure 2).

First, under hydrostatic pressure, the crack ends generated by the initial impact can remain open. Assuming that the hydrostatic pressure remains constant along the X direction

and is not affected by the crack width, the pressurized water fills the entire crack length L_w . Because the cracks produced by damage and failure are mainly type I cracks, cracks will produce displacement perpendicular to the crack surface under the action of tensile stress perpendicular to the crack surface. Under this assumption, the quasi-static type I stress intensity factor of crack tip is¹¹

$$K_I = 2\sqrt{\frac{r_0 + L_w}{\pi}} \int_0^{r_0 + L_w} \frac{P_{\max}}{\sqrt{(r_0 + L_w)^2 - x^2}} dx \quad (7)$$

where K_I is type I stress intensity factor, $N/m^{3/2}$; r_0 is the drilling radius, m; L_w is the crack length, m.

According to the classical model of fracture mechanics, when the crack length L_w is much larger than the bore hole radius r_0 , the round hole can be regarded as a part of the crack. Under this model, type I stress intensity factor can be expressed as²⁸

$$K_I = \sqrt{\pi a} \sigma_y \quad (8)$$

where a is the overall crack length, $a = r_0 + L_w$, m.

$$\sigma_y = 2 \int_0^{r_0 + L_w} \frac{P_{\max}}{\sqrt{(r_0 + L_w)^2 - x^2}} dx \quad (9)$$

According to eq 9, under the same peak pressure, the stress value σ_y in the Y direction of the crack tip will gradually decrease with the increase of the crack length. The crack will continue to expand if σ_y is greater than the tensile strength of the crack. When σ_y is lower than the tensile strength of the crack, the crack stops growing.

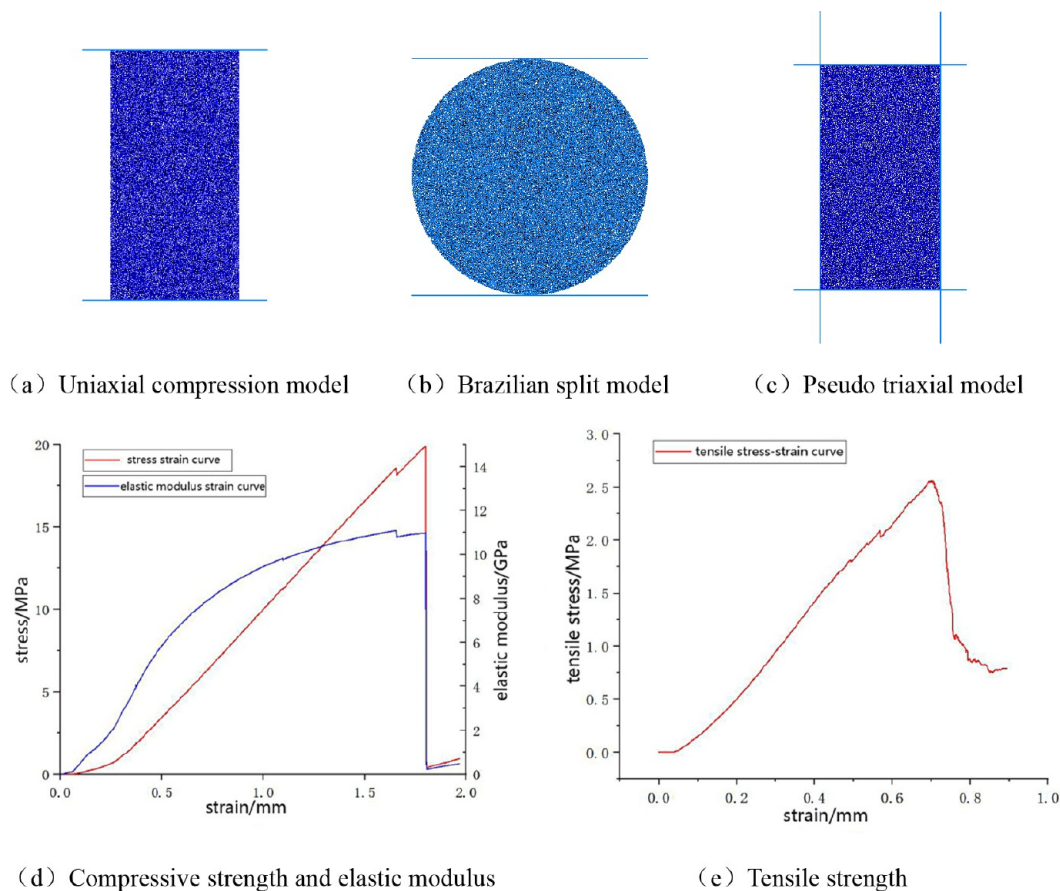
2.2. Establishment of Numerical Model. First, the Particle Flow Code software (PFC^{2D}) was used to conduct the numerical calculation of coal caused by hydraulic electric pulse in drilling, and analyze the crack propagation, morphological characteristics, and crack propagation law.

2.2.1. Determination of Numerical Model Parameters. In PFC^{2D}, the simulation material is composed of discrete rigid ball elements and different types of bonding bonds between balls. Among these different types of bonding bonds, the parallel bond (PB) can transfer the forces and torques between the ball elements. The bond fracture in the PB model will lead to a significant reduction in stiffness,²⁹ which will affect the microscopic stiffness of adjacent particles and the overall macroscopic stiffness of the material. This is quite consistent with the property that the strength of rock decreases with the crack growth, so the PB model is adopted in this model. To define a PB model material, a set of contact microparameters must be defined first, which includes linear equivalent modulus E^* , linear shear stiffness $\kappa^* = \frac{k_n}{k_s}$, viscous equivalent modulus \bar{E}^* , viscous shear stiffness $\bar{\kappa}^* = \frac{k_n^*}{k_s^*}$, cohesion \bar{c} , tensile strength $\bar{\sigma}_c$, friction angle $\bar{\varphi}$, and friction coefficient μ . These parameters need to be determined by establishing different models through PFC^{2D}, and then comparing the results with the macroscopic physical and mechanical parameters of the experimental coal samples, and finally determining the contact microparameter. The specific practices are as follows.

The model adopted in the numerical calculation in this paper is based on the laboratory test coal sample, which is taken from No.3 coal seam of Sihe Coal Mine, Jincheng, China. The coal sample is anthracite with uniform structure, large hardness, and

Table 1. Physicomechanical Parameters of the Coal

Rock type	Tensile strength/MPa	Compressive strength/MPa	Elastic modulus/GPa	Poisson's ratio/ μ	Cohesion/MPa	Internal friction angle/(deg)
coal	2.53	19.69	11.07	0.30	1.78	35

**Figure 3.** Schematic diagram of simulation.

typical geological units. The specific physicomechanical parameters of the coal sample are shown in Table 1.

To make the macroscopic properties of simulated material the same as coal samples, PFC^{2D} is used to build the uniaxial compression model, the brazilian splitting model, and the pseudo-triaxial model, as shown in Figure 3(a–c). Through the above three-simulation test to verify the mechanical properties of the material, and after many times of trial and error adjustment, the contact microparameters that need to be set during model establishment are finally obtained as shown in Table 2.

In the process of determining the contact microparameter of the model, the physical and mechanical parameters of the

Table 2. Contact Microparameters

Microparameter	Value in numerical calculation
Linear equivalent modulus E^*/GPa	1.2
Rigidity of linearity κ^*	20
Viscous equivalent modulus \bar{E}^*/GPa	2.4
Viscosity stiffness ratio $\bar{\kappa}^*$	15
Cohesion \bar{c}/MPa	40
Tensile strength $\bar{\sigma}_t/\text{MPa}$	19.8
Friction angle $\bar{\varphi}/(\text{deg})$	35
Friction coefficient μ	0.38

simulated materials were obtained by the simulation. The loading rate is according to the current standard *Test Method Standard for Engineering Rock Mass* (GB/T 50266–2013),³⁰ the loading rate of 1 MPa/s is adopted in the uniaxial compression test. In the pseudotriaxial loading simulation, after the confining pressure reached the preset value at the loading rate of 0.5 MPa/s, then the axial pressure was applied at the loading rate of 1 MPa/s until the specimen was damaged. Finally, to verify the stability of the microparameters, five groups of specimens were randomly generated for each simulation. The calculation results of the first group were shown in Figure 3(d,e).

The physical and mechanical parameters of the final model materials of the five groups were shown in Table 3. There is little difference between the data obtained by numerical simulation and the data measured in the laboratory, which means that the microparameter can be used in the numerical calculation model.

2.2.2. The Establishment and Loading of Numerical Model. It is verified that the macroscopic properties of the PFC^{2D} model established by using the microparameter (shown in Table 2) are basically consistent with the micromechanical parameters measured in the laboratory. Therefore, the microparameter in Table 2 is used to establish the model. The model size is 30 cm \times 30 cm, and the diameter of the central water injection hole is 26 mm. To simulate the mechanical boundary conditions of the coal, the

Table 3. Comparison of Basic Properties between Laboratory and Simulated Material

Rock type	Tensile strength/MPa	Compressive strength/MPa	Elastic modulus/GPa	Poisson's ratio μ	Cohesion/MPa	Internal friction angle/(deg)
Laboratory data						
coal	2.53	19.69	11.07	0.30	1.78	35
Simulated data						
1	2.53	19.91	11.08	0.31	1.81	36.23
2	2.54	19.53	11.12	0.29	1.80	37.01
3	2.55	19.47	11.07	0.31	1.77	34.65
4	2.56	19.78	11.03	0.30	1.79	32.77
5	2.53	19.59	11.21	0.30	1.80	34.50
average	2.54	19.66	11.10	0.30	1.79	35.03
Difference value/%						
	+0.39	-0.15	+0.27	+0.66	+0.56	+0.09

horizontal confining pressure of the coal samples applied is 8.66 MPa (Figure 4).

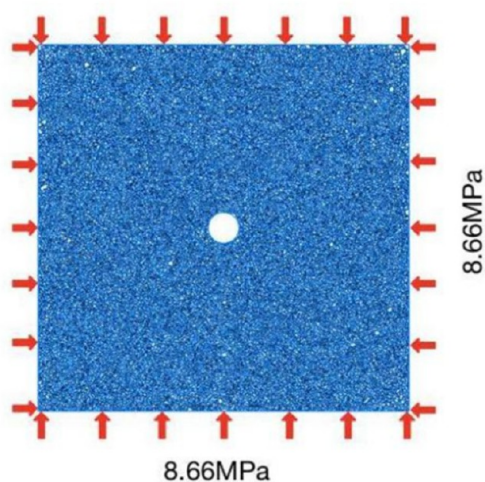


Figure 4. Model loading diagram.

To load the coal model in simulation, a water shock wave waveform under different water pressure and discharge voltage conditions should be obtained by test. Therefore, a water shock wave loading test is carried out in the laboratory first. The test system consists of a high-voltage electrical pulse discharge system, a pipeline bearing system, and a water shock monitoring system (Figure 5). The high-voltage electrical pulse discharge system consists of high voltage electric pulse power supply (capacitor box, discharge switch, etc.), cable, discharge electrode, etc. The pressure tube is connected by flanges. The length of the pressure pipe can be changed by removing the flanges. The system can test the water shock pressure value by a water shock monitoring system where a high frequency pressure probe (connected with the dynamic data storage recorder) is placed on the pressure pipe to collect the water shock signal.

After the electrode discharged in water, water shock waves are formed. A high frequency pressure probe is used to collect the information on water shock wave waveform. Take the first pressure pulse waveform as one of the most representative waveform, and the water shock waveforms under the condition of 9 kV, 11 kV, and 13 kV discharge voltage on the basis of 3 MPa hydrostatic pressure are as shown in Figure 6.

The stress wave data measured by the above water shock monitoring system are assigned to the middle water injection hole wall at a frequency of 10^7 Hz to simulate the impact of water

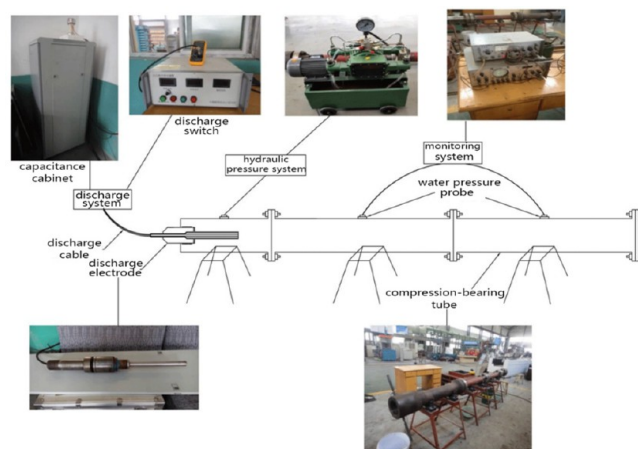


Figure 5. Water shock test system.

shock waves on the hole wall of coal. The PFC^{2D} fluid code was used to set the fixed water pressure of the water injection hole as 3 MPa. To verify the correctness of the loading method, the pressure of the water injection hole wall and the imported stress wave are monitored. Figure 7 shows the relationship between the pressure of the water injection hole wall and the imported stress wave monitored in the first discharge under the condition of 3 MPa + 9 kV (where green is the imported stress wave and red is the monitored pressure of the water injection hole wall). The pressure wave of the simulated water injection hole is highly consistent with the imported stress wave, which also means that the method is feasible.

2.3. Analysis of Numerical Simulation Results.

2.3.1. Qualitative Analysis of Crack Morphology. The results of crack propagation in coal after 10 times of three different load combinations are shown in Figure 8.

From Figure 8, the crack develops along the radial direction of the injection hole and spreads radially. From Figure 8(a), under the discharge condition of 9 kV, four main cracks appear around the borehole of coal, the number of microcracks around the borehole is small, and no failure area is formed around the borehole. The length of the four main cracks is relatively uniform, the average length of the cracks is 46.6 mm. Under the discharge condition of 11 kV, seven main cracks appeared around the borehole of coal, and the length of the main cracks increased significantly. The average length of the crack was 109.4 mm, and the crack direction was clear. The number of microcracks around the borehole increased and a microcrack network was formed, and a relatively obvious failure area was formed around the borehole (Figure 8(b)). Under the discharge

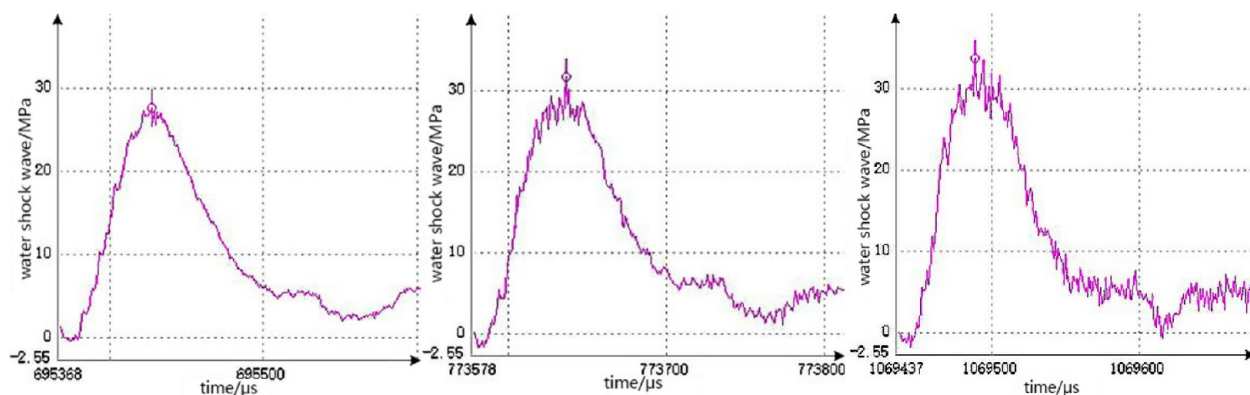


Figure 6. Water shock pulse pressure diagram.

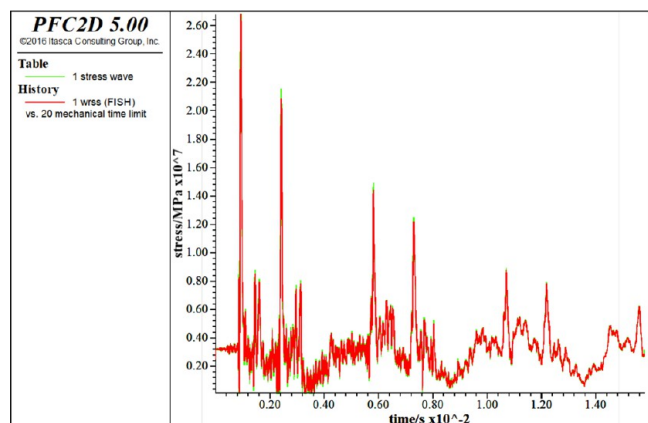


Figure 7. Loading diagram of coal samples.

condition of 13 kV, seven main cracks appear around the coal borehole. The crack direction is clear, and the crack extension length and tortuous degree are further increased. Three of the main cracks were close to the boundary of the model, and one main crack reached the boundary of the model. The average length of the crack was 155.6 mm, and the crack propagation was sufficient. The number of microcracks around the borehole increased significantly and formed a microcrack network, forming a large failure area (Figure 8(c)).

From Figure 8, with the increase of discharge voltage, the length and number of the main crack and microcracks increase significantly. The bending and torquing degrees of the main

crack increase significantly. The microcrack network around the borehole becomes more and more complex, and the damage area around the borehole becomes larger and larger. Under different voltages, the main cracks are alternately long and short. This phenomenon indicates that under the action of a water shock wave, the adjacent crack growth will appear to be under the stress interference phenomenon, resulting in the alternating occurrence of long and short cracks in the crack growth.

2.3.2. Quantitative Analysis of Crack Damage. The damage variable can quantitatively characterize the deterioration degree of coal. It is an internal state variable and a field variable that can objectively reflect the internal damage characteristics of coal. In the numerical model, when the bond between two ball elements is broken, it is considered that microcracks are generated between the balls. In Figure 9(a), the blue bond represents the effective bond, and red is the failed bond. The total bond number around the hole with a diameter of 80 mm (about 3 times the diameter of the hole) is extracted as N , and the number of broken bonds is extracted as N_a . Then the damage variable of coal can be defined as

$$D_n = \frac{N_a}{N} \quad (10)$$

where D_n is the damage variable; N_a is the number of damaged microcracks; N is the total bond number.

Combined with the numerical model calculation results and eq 10, the damage variable values under different discharge voltages and discharge times can be obtained (Figure 9(b)).

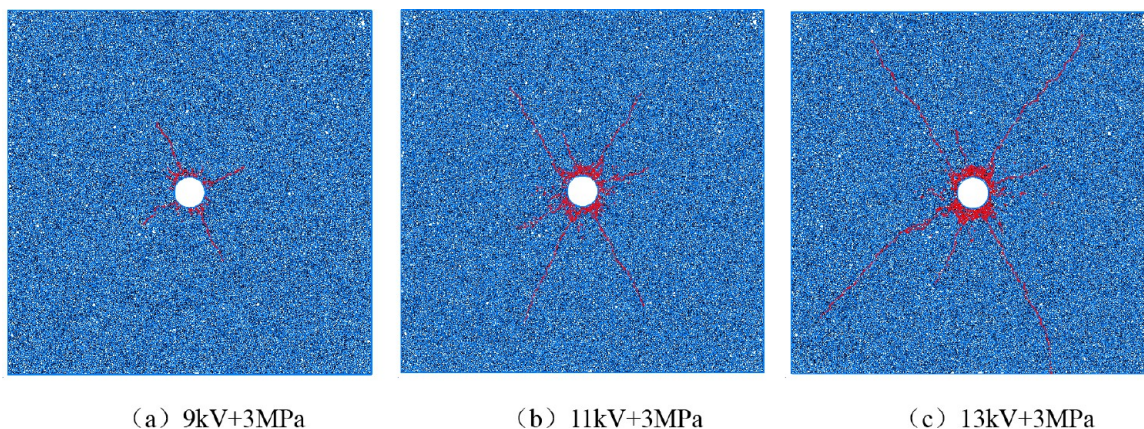


Figure 8. Crack distribution under different load combinations.

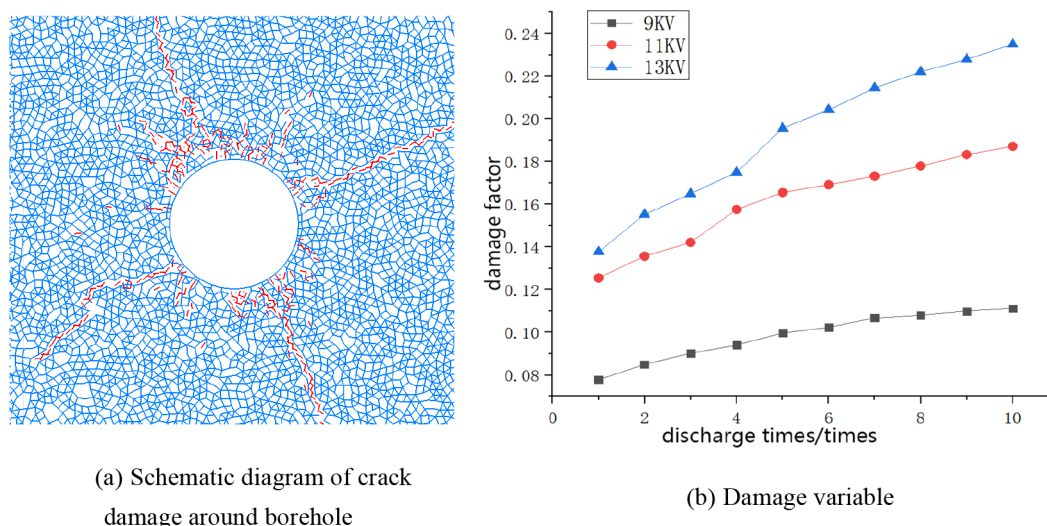


Figure 9. Damage and damage factors around borehole.

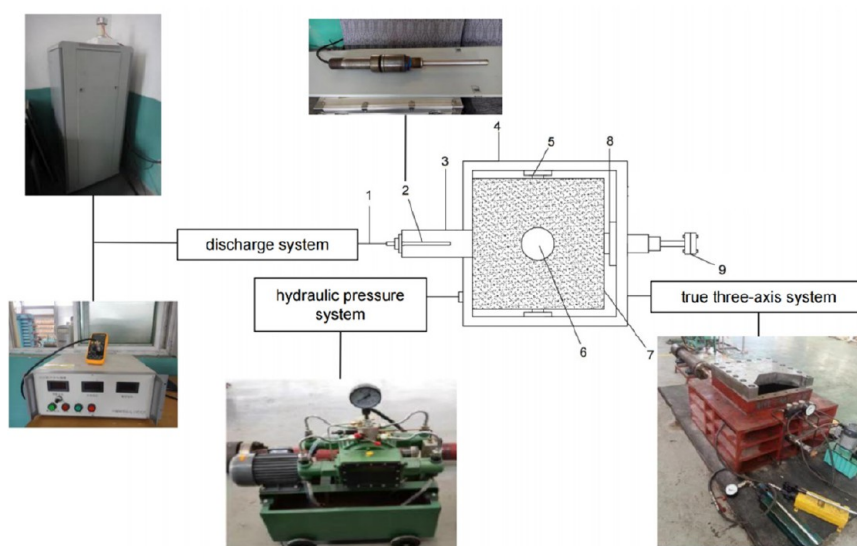


Figure 10. High-voltage electrical hydraulic fracturing test platform.

Figure 9(b) shows that the trends of the coal damage variable under the condition of different voltage discharges are similar. The trend increased with the increase of discharge voltage and discharge times. The coal degradation increased with the increase of discharge voltage and increase of discharge times. The microcracks in the coal are constantly starting, expanding, and finally penetrating. Under the same discharge voltage condition, the growth rate of damage variable experienced a rapid increase stage, and a sharp increase stage (3–6 times discharge), and then gradually slowing stage with the increase of discharge times. Through this phenomenon, the crack propagation of hydraulic electric impulse load impacting coal can be divided into three stages: ① Damage accumulation stage: in the early stage of crack initiation, the microcracks around the borehole and the damage accumulated increase rapidly. ② Main crack growth stage: when the damage around the borehole accumulates to a certain extent, the water shock wave will break through the weak point and expand along the radial direction to form several main cracks, and the damage increases sharply. ③ Multicrack competitive growth stage: the rapid growth of one

main crack will affect the growth of the surrounding cracks, resulting in a competitive growth relationship with the adjacent cracks. The growth of the main crack is slowed and the damage of the coal is slowed also.

3. PHYSICAL TEST AND CT IMAGE DATA ACQUISITION

Although the above numerical results prove that the high voltage electric pulse increasing permeability technology is an effective artificial fracture forming technology, considering the complexity of the structure and force in coal, to further analyze and study the fracture damage expansion and morphology distribution law of the natural coal reservoir, a hydraulic electric pulse physical test on the coal was carried out.

3.1. Test Equipment and Test Coal Samples. The high voltage electric pulse hydraulic fracturing test platform is mainly composed of the following: high voltage electrical pulse discharge system and loading system (Figure 10), and a high voltage electrical pulse discharge system which consists of the following: coaxial transmission cables 1, discharge electrode 2,

and pressure pipe 3. The loading system consists of a rigid triaxial pressure chamber 4; ultrathin jack 5, 6; a hollow jack 8; coal specimens 7; and end flange 9; etc.

3.2. Test Plan. The test should meet the similarity law in space: the geometric similarity ratio is 1:20, the simulated coal seam with 5.7 m thickness in the coal mine site, the similarity ratio of loading stress is 1:1, the similarity ratio of water pressure in the borehole is 1:1, the similarity ratio of bulk density is 1:1, and the similarity ratio of strength is 1:1.

Before the test, the original coal sample (1# specimen) was selected for drilling and sampling with a diameter of 80 mm, and then the CT scan of the drill core was conducted to study the distribution of cracks in the raw coal sample. Then, the 2#–4# specimens were put into the triaxial pressure chamber in turn, and the coal samples were subjected to triaxial loading. The vertical loading was 7.28 MPa, and the horizontal confining pressure was 8.66 MPa. After the confining pressure was loaded on the specimen, a hydrostatic pressure of 3 MPa was applied to the specimen through the pressure pipe and kept unchanged, and a high voltage discharge of different voltages was carried out. The specific test scheme is shown in Table 4.

Table 4. Hydraulic Fracturing Procedures of High Voltage Pulse Discharge

Specimen no.	Triaxial stress/MPa			Water pressure/MPa	Voltage/kV	Discharge times
	σ_v	σ_H	σ_h			
1#	0	0	0	0	0	0
2#	7.28	8.66	8.66	3	9	10
3#	7.28	8.66	8.66	3	11	10
4#	7.28	8.66	8.66	3	13	10

After the test is completed, the Z1Z(W)–200E universal engineering drilling rig is applied to take a drill core with a diameter of 80 mm along the original central drilling direction for sampling (Figure 11). Then, CT section scanning was conducted on the specimen drill core to study and analyze the fracturing effect of the coal samples.

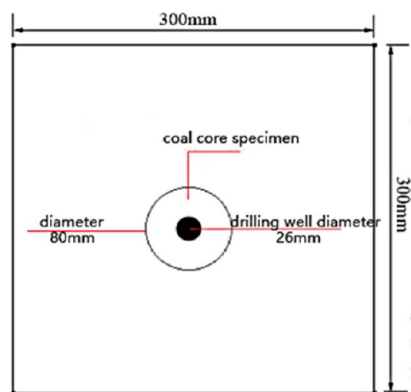


Figure 11. Drilling core sampling plan.

The 225CT KVFCB micro-CT experimental system was used to conduct CT scanning of the coal cores (Figure 12). Without changing the original state of the specimen, the layered scanning of its internal structure can analyze the distribution of pores, cracks, and density changes of each layer image, and provide

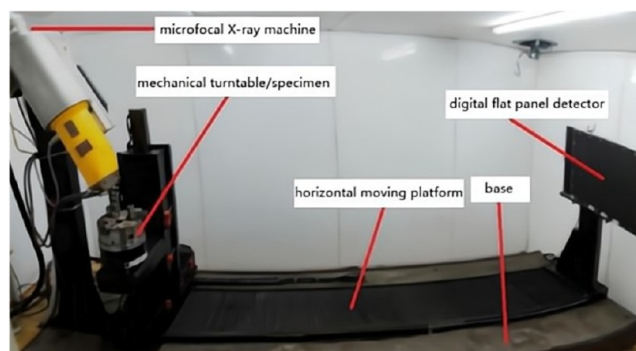


Figure 12. Industrial CT scanning equipment.

accurate internal information data for the subsequent establishment of a three-dimensional reconstruction model.

CT scan results are obtained after CT scanning, filtering, and reconstruction of coal drill cores. About 1500 CT images can be obtained for each drill core, and some results are shown in Table 5.

From Table 5, there are little cracks in the 1# specimen (the original coal sample); their width is small and length is short. Under different loading conditions, many cracks of different lengths and widths are generated on the coal samples of 2#, 3#, and 4#. The number, length, width, and density of cracks increase with the increase of discharge voltage and energy. Most of the cracks started from the periphery of the drilling hole and extended to the edge of the drilling core. The higher the voltage was, the more fully the crack spread.

By comparing the crack distribution and morphology of specimens 2#, 3#, and 4# with the numerical simulation results, the number of cracks in both numerical simulation and test tended to increase with the increase of discharge voltage. Observing the crack trend, most of the cracks in the 2#, 3#, and 4# specimens spread outward in the radial direction from the borehole wall. The distribution of cracks in morphology is highly similar between the numerical simulation results and the test results, and the numerical simulation represents well the prediction and trial and error of the test.

4. THREE DIMENSIONAL RECONSTRUCTION OF COAL

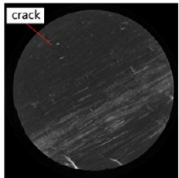
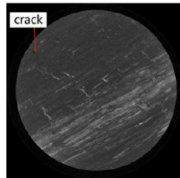
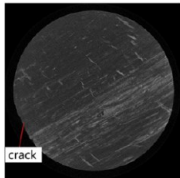
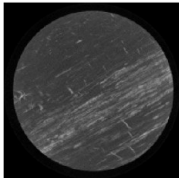
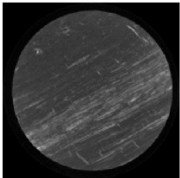
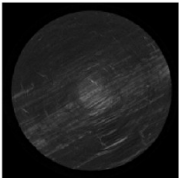
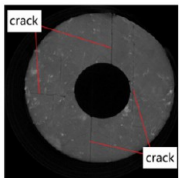
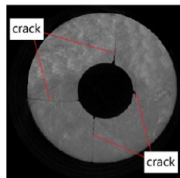
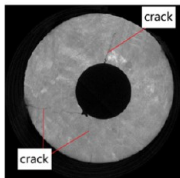
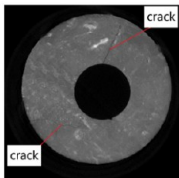
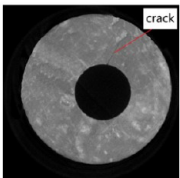
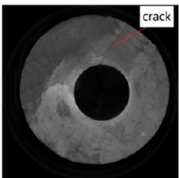
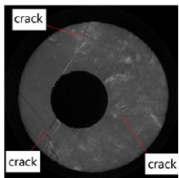
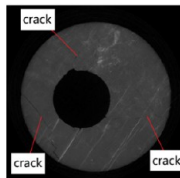
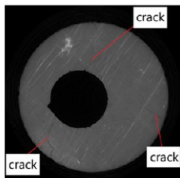
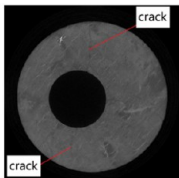
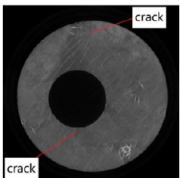
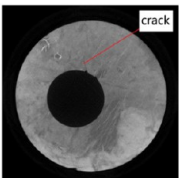
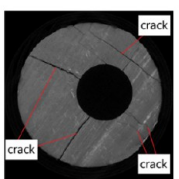
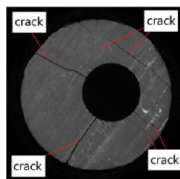
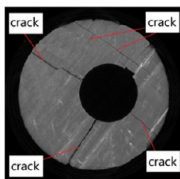
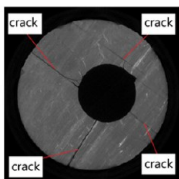
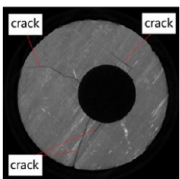
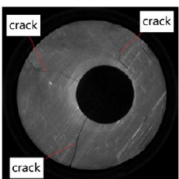
Due to the size of coal core and the planarity of CT scan images, it is necessary to reconstruct the coal core crack in three dimensions, and further study the spatial location, morphology, and propagation law of the crack.

The 3D reconstruction technology of coal needs the help of certain computer software or advanced mathematical algorithms. In this paper, Mimics software is used to recombine CT images into a personal data set to form the reconstructed 3D model.

4.1. Crack Morphology Analysis after Hydraulic Fracturing with High Voltage Electric Pulse. When the transparency of the matrix mask is adjusted to the maximum, and the crack is adjusted to the opacity, the 3D reconstruction perspective of raw coal and coal drill core under three different load conditions can be derived (Figure 13). The gray part with high transparency represents the coal matrix, and the green part with opacity represents the crack.

The structure and distribution of cracks inside the coal core specimen can be clearly observed in Figure 13. The 1# specimen is the original coal sample without loading (Figure 13(a)). The 2# specimen mainly has two cracks running from the top to the

Table 5. CT Scan Results of Coal Samples at Different Discharge Voltages

Specimen number	100 layer	300 layer	600 layer	900 layer	1200 layer	1490 layer
1#						
2#						
3#						
4#						

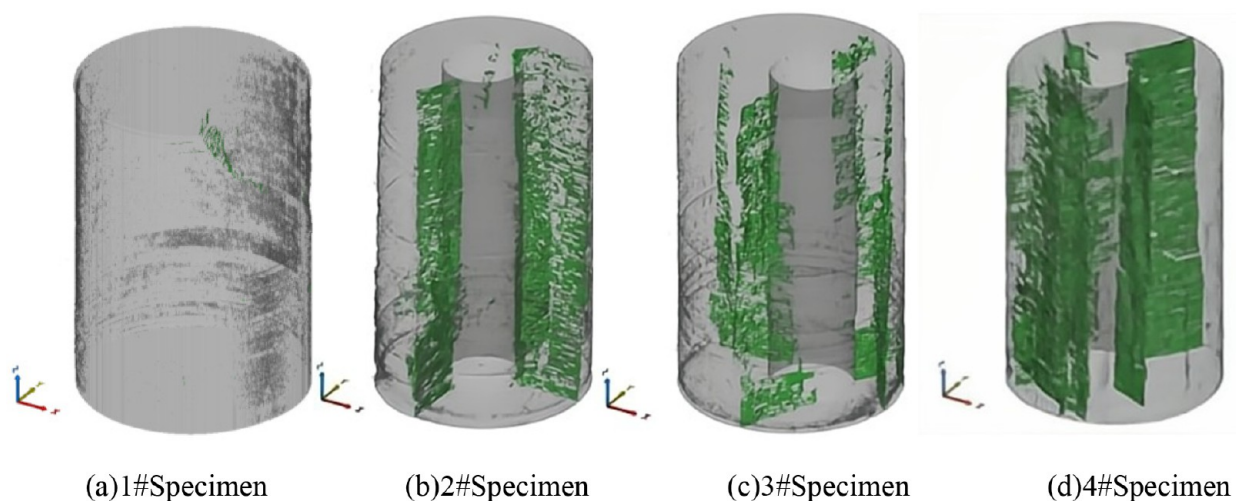


Figure 13. Perspective view of three-dimensional cracks in the core of different specimens.

bottom, which are distributed in the relative direction along the borehole (Figure 13(b)). The crack network of the 3# specimen is more complex than of the 2# specimen. The cracks are distributed intermittently at different angles along the borehole, and the density of the small cracks composing each flake crack is relatively small. The crack network structure of specimen 4# is

the most complex, and a large core damage area is formed by the intersection of multiple cracks, where the cracks are directly connected from the top to the bottom.

To observe the structural morphology of cracks in each coal core specimen more clearly and specifically, according to the distribution and connectivity of cracks in the space of the coal

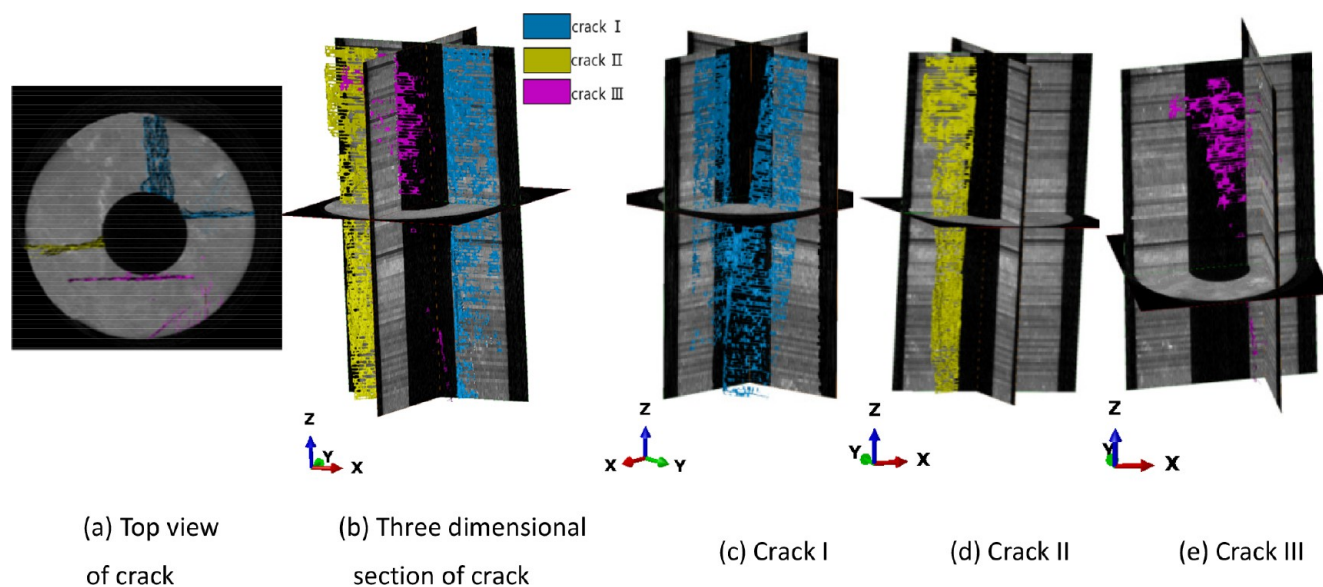


Figure 14. Top view of the 2# sample crack and the overall and partial three-dimensional slices.

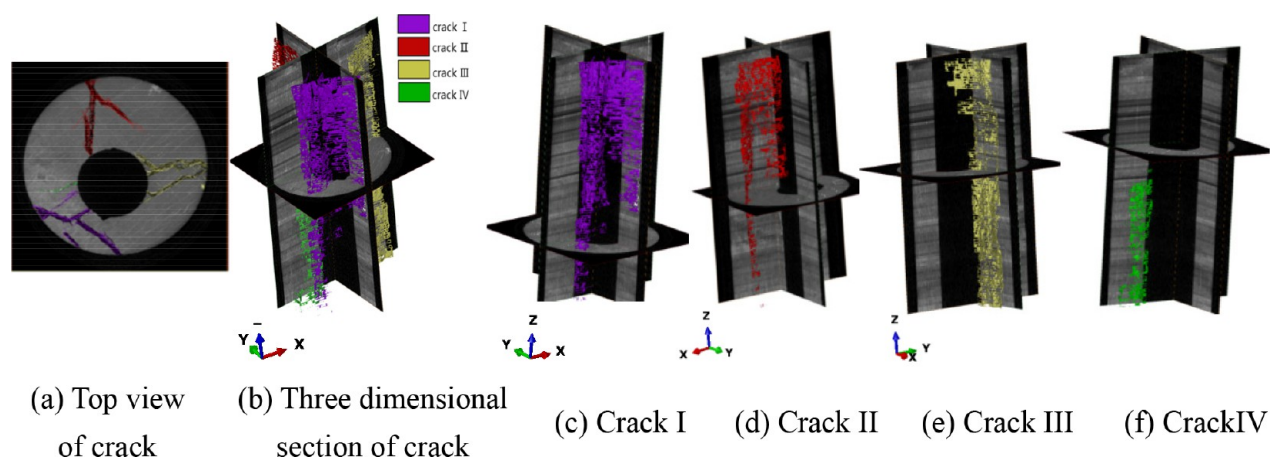


Figure 15. Top view of the 3# sample crack and the overall and partial three-dimensional slices.

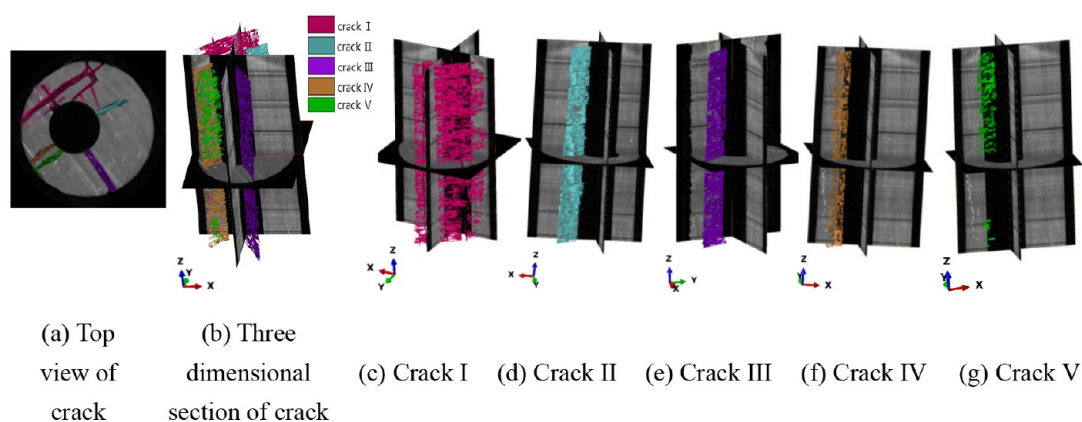


Figure 16. Top view of the 4# sample crack and the overall and partial three-dimensional slices.

core specimen, the cracks were divided into different zones and marked with different colors one by one, and then the three-dimensional sections of the model were adjusted to appropriate angles and positions. The top view of each specimen, the three-dimensional section diagram of the whole crack, and the three-

dimensional section diagram of each crack region were extracted, respectively (Figure 14, Figure 15, and Figure 16).

Figure 14 shows the top view of cracks (Figure 14(a)), 3D section of cracks (Figure 14(b)), and the three wing crack extensions in the 2# specimen by the hole edge: blue crack I (Figure 14(c)), yellow crack II (Figure 14(d)), and pink crack

III (Figure 14(e)). These cracks are composed of numerous microcracks, and their distribution range, area, volume, and morphology are different. Crack I and crack II started from the edge of the central drilling hole and developed to the edge of the specimen. Crack III was a crack parallel to the tangent direction of the drilling hole. It can be seen from Figure 14(c) that crack I is a “V” shaped crack, which runs from the top to the bottom of the specimen. The vertical bifurcating angle of the V shape in the vertical direction is 14.13° , and the horizontal bifurcating angle of the V shape in the upper part of the coal core specimen gradually decreases from 91.05° . This indicates that the shock wave first acts on the top of the coal core and carries a large amount of energy. As the shock wave propagates to the bottom of the specimen, the energy gradually decreases, and the confluence of crack I occurs. Compared with crack I, crack II is simpler in form, which is directly connected from the top to the bottom of the coal core. However, the horizontal width of the middle and upper part of the crack is larger than that of the lower part, and the crack presents a state of “wide at the top and narrow at the bottom”. Crack III exists in a small area and is not connected up and down. It appears in the middle and upper part of the coal core specimen, and there are only a few microcracks in the lower part. The crack initiation and propagation are related to the distance from the discharge electrode, which also causes the complexity of crack space morphology and distribution.

Figure 15 shows the top view of cracks (Figure 15(a)) the 3D section of cracks (Figure 15(b)) and 4 main cracks in the 3# specimen, among which the main cracks I, II, III, and IV extend from the hole edge to the edge of the coal core with full expansion and complex spatial network. Cracks I and III are basically connected in the vertical direction, while cracks II and IV are discontinuously distributed in the vertical direction. Crack IV only exists in the middle and lower part of the core, the end face of the specimen is not visible, and its area and length are small. The purple crack I (Figure 14(c)) and the red crack II (Figure 14(d)) were basically similar in shape, with a shape of “wide at the top and narrow at the bottom”, but the area, volume, and density of crack I were slightly larger than that of crack II.

Combined with the top view of the cracks (Figure 15(a)), it can be found that both cracks I and II have bifurcation. Crack I is a main crack of an arc with branch cracks on both sides, and the whole crack looks like a Y shape, while crack II presents a bifurcation phenomenon of V shape, with a bifurcation angle of 37.51° . The yellow crack III (Figure 15(e)) was vertically connected from the top to the bottom, in the shape of V, but slightly curved with a small angle of 26.57° . The green crack IV (Figure 15(f)) is a nonpenetrating crack that only exists in the middle and lower part of the coal core specimen. It is distributed around crack I with small extension length, area, and volume, and extends outward from the borehole but does not extend to the edge of the specimen.

From Figure 16, by the top view of crack and 3D section of crack, it can be seen that the 4# specimen has 5 crack distribution regions, and each part has a different spatial connectivity. Among these cracks, the pink crack group I (Figure 16(c)) has a complex structure with interwoven cracks. Two main cracks extending outward from the edge of the drilling hole bifurcate, expand, and converge into another main crack parallel to the tangent direction of the drilling hole, and the overall shape is “H”. Each main crack has several branch cracks, and the crack group penetrates from the top of the coal core specimen to the bottom, with good vertical penetration, which is conducive to

coal-bed methane overflow. The morphology of blue crack II (Figure 16(d)), purple crack III (Figure 16(e)), and yellow crack IV (Figure 16(f)) is basically the same. All of them extend outward from the edge of the borehole and can be penetrated from the top of the coal core specimen to the bottom, without crossover and bifurcations. Compared with crack I, they are simple in morphology. The green crack V (Figure 16(g)) is distributed in parallel with crack IV, which mainly exists in the middle and upper part of the coal core specimen.

In conclusion, the macroscopic cracks of coal caused by high voltage electric pulse are formed by the concentration of small cracks, and the small cracks are formed by the evolution and agglomeration of smaller cracks. Under the condition of 3 MPa hydrostatic pressure, when the discharge voltage is 9 kV, there are two main cracks in the coal core, which are independent of each other. When the discharge voltage is 11 kV, the main cracks increase to four, and the cracks are in a through-through and intermittent distribution. When the discharge voltage increases to 13 kV, the number of main through-through cracks in the coal core increases to five, among which there is a crack group with complex shape (crack I), the crack area increases significantly, and the degree of complexity further increases. The higher is the discharge voltage, the greater is the number of main cracks and small branches. The larger are the crack area and volume, the more complete is the crack development, and the higher is the damage degree, forming a crack network of a certain scale, which provides a good space environment for the permeability and migration of coal-bed methane.

4.2. Analysis of Fracture Rate and Damage Characteristics in Coal.

4.2.1. Evaluation and Analysis of Damage Factors and Fracture Rate.

The above research of hydraulic electrical pulse fracturing of coal crack effect and crack propagation, distribution, shape law, has carried on the qualitative analysis and study. For further quantitative study of spatial structure characteristics and the internal cracks of coal damage characteristics, this paper will continue to study the damage of coal after cracking by introducing damage factors and fracture rate. The total cross-sectional area crack group, crack surface area, coal core volume, and crack volume cracks in each specimen can be obtained by Mimics software statistics, as shown in Table 6.

Table 6. Total Cross-Sectional Area Crack Group, Crack Surface Area, Coal Core Volume, and Crack Volume in the Specimens

Specimen number	Crack surface area/mm ²	Total areas of all crack groups/mm ²	Volume of crack/mm ³	Coal core volume/mm ³
2#	38379.53	255673.32	3182.85	1497395.13
3#	54666.93	309450.07	3603.47	1450374.66
4#	88070.27	373940.31	8777.05	1442720.33

(1) Damage factor D_A defined by crack surface area damage:³¹

$$D_A = A_D/A \quad (11)$$

where A_D is the damage area formed under external load, namely crack surface area; A is the original surface area of coal core.

(2) Damage factor D_V defined by crack volume damage:

$$D_V = V_D/V \quad (12)$$

where V_D is the damage volume formed under external load; V is the original volume of coal core.

The damage factors of each specimen can be obtained by substituting the data in Table 6 into eqs 11 and 12, and the variation of damage factors with voltage can be plotted, as shown in Figure 17.

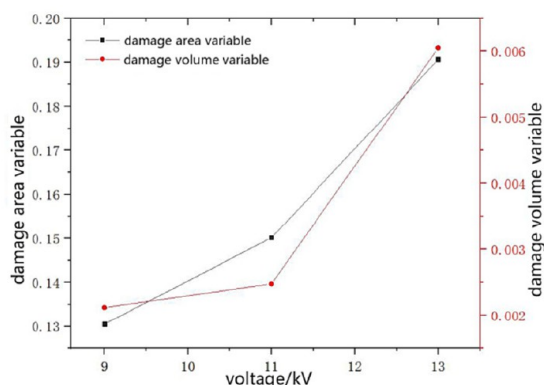


Figure 17. Damage factor of each specimen area and volume.

From Figure 17, the crack area and volume damage factors increase with the increase of voltage, which is consistent with the numerical simulation results. When the voltage changes from 9 kV to 11 kV, the change rate of the damage factor is relatively small. The change rate of the area damage factor with voltage is 0.98%, and the change rate of the volume damage factor with voltage is 0.018%. When the voltage changes from 11 kV to 13 kV, the two damage factors are significantly improved in value. The area damage factor changes with voltage at 2.02%, which is about 2 times higher than that of the former, and the volume damage factor changes with voltage at 0.18%, which is 10 times higher than that of the former. This indicates that discharge voltage has a great influence on the damage and crack structure of coal, especially on the crack volume.

The damage factors represent the overall internal damage of coal. To further refine the damage azimuth in the actual coal-bed, methane pumping work is used to determine the coal-bed methane seepage channel. To explore the distribution of cracks in different directions of coal after fracturing by high-pressure electric pulse water pressure, the top view obtained after 3D reconstruction was imported into PCAS software to obtain the numerical value of the crack rate in each angle and draw the corresponding rose diagram (Figure 18).

Figure 18 shows that the crack rates of the three specimens in each direction are different, and the number of angles distributed are also quite different. Crack networks of different complexity

are formed in coal under different voltage loading conditions. There were 18 statistical azimuth angles of cracks in specimen 2#, and the cracks were mainly distributed in the 305°–308° and 115°–245° regions. The maximum crack rate at 170°–190° was 0.6474, and the crack rate at the other directions was smaller, ranging from 0.0874 to 0.2859. The average fracture rate was 0.247. The number of crack azimuth angles of the 3# specimen is 11, among which the crack rate of 6 angle directions is greater than the average crack rate of the 2# specimen, and the average crack rate of the 3# specimen is 0.298. The cracks of the 4# specimen (Figure 18(c)) had up to 20 statistical azimuth angles, and the maximum crack rate was 0.579, which ranged from 300° to 310°. Other cracks showed a 360° uniform distribution, with an average crack rate of 0.217. Figure 18 shows, with the increase of discharge voltage, the first crack inside the coal was a symmetrical two-angle centralized crack, which gradually formed a concentrated distribution in the direction of the development of the small angle. Finally, there was a 360 deg ring with divergent shape distribution, forming the angles of the crack network. The results are extremely beneficial to the practical engineering of coal-bed methane in the infiltration and circulation applications.

4.2.2. Evaluation and Analysis of Fractal Dimension. To analyze the geometric distribution characteristics of cracks in coal and the complexity of the distribution of the correlation network between cracks and fracture characteristics, fractal dimension d is introduced. Generally, cracks with fractal dimension d between 1 and 3 have good fractal characteristics.³² The larger the value of d is, the more the shape of the microfractures will be bent, and the more fracture networks will be formed when they are connected with each other.

The box dimension calculation method is used to define d : a square lattice ($\delta \times \delta$) is used to cover the point set composed of cracks, and the size of the box is adjustable. In this paper, the total number of boxes $N_i(\delta_i)$ needed to cover the point set composed of cracks is calculated by taking $\delta = 2$ mm. Assuming that the lattice covering $\delta_i \times \delta_i$ at step i is covered, the number of boxes required is $N_i(\delta_i)$, and the lattice (δ_{i+1}) \times (δ_{i+1}) required at step $i+1$, the number of boxes $N_{i+1}(\delta_{i+1})$ is required. When different values of i are taken, the value of N_i will change accordingly, which conforms to the three-dimensional surface with fractal geometric characteristics, and its rule is as follows:³³

$$\frac{N_{i+1}}{N_i} \sim \left(\frac{\delta_i}{\delta_{i+1}} \right)^d \quad (13)$$

Namely:

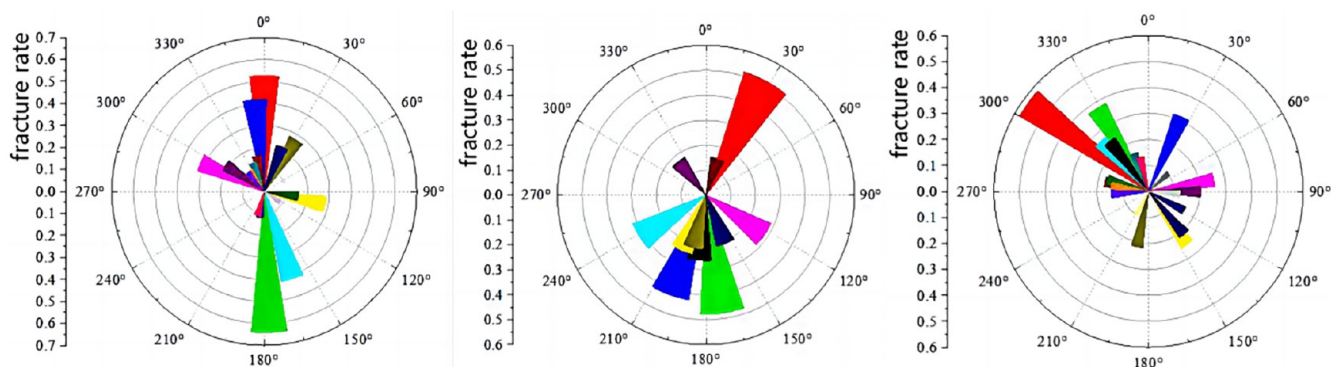


Figure 18. Rose diagram of the distribution of the crack rate of each specimen at different angles.

$$\log\left(\frac{N_{i+1}}{N_i}\right) = d \cdot \log\left(\frac{\delta_i}{\delta_{i+1}}\right) + b \quad (14)$$

In the Mimics 3D reconstruction software, the surface areas of crack groups of 2#, 3#, and 4# specimens were derived, respectively, then the corresponding $\log(\delta_i/\delta_{i+1})$ and $\log(N_{i+1}/N_i)$ were obtained. Finally, origin software was used to fit and calculate all the statistical results in turn to obtain the fractal dimension d . The statistical results of the fractal dimension of each crack group were shown in Table 7, and the fitting diagram of the overall fractal dimension of each specimen was shown in Figure 19.

Table 7. Statistical Results of Fractal Dimension of Each Crack Group

Specimen no.	Frack group	Superficial area/ mm ²	Fractal dimension/d
2#	I	21275.07	1.996
	II	12950.57	2.012
	III	4053.59	1.889
	Overall specimen	38379.53	2.017
3#	I	17522.78	1.996
	II	9835.09	1.983
	III	20737.66	1.997
	IV	5879.35	1.974
	Overall specimen	54666.93	2.013
4#	I	43177.7	1.997
	II	13413.4	1.96
	III	19211.05	1.97
	IV	3790.35	2.133
	V	8470.33	2.071
	Overall specimen	88070.27	1.995

From Table 7, the fractal dimension of crack groups in all specimens is between 1 and 3, and fluctuates around 2. The fractal dimension of all crack groups of specimen 2# is maintained between 1.889 and 2.017, with an average value of 1.979. The minimum value is 1.889 of crack III, which is the smallest fractal dimension of the crack group in all specimens. By comparing the reconstruction results, 2# crack III (Figure 14(e)) has a flat crack surface and a flake crack group with a simple network structure. The fractal dimension values of each crack group in 3# are between 1.974 and 2.013, with an average value of 1.993. The fractal dimension of each crack group in 4# is maintained between 1.96 and 2.133, with an average value of 2.012 and a maximum value of 2.133 of crack IV, which is the largest among all specimens. Comparing the reconstruction results, specimen 4# crack IV (Figure 16(f)) has a complex microcrack network structure with intersecting microcracks and torturing crack surfaces. The average fractal dimension of crack groups in each specimen increases with the increase of discharge voltage, and the number of microcracks in each crack group, the degree of crack propagation branching into a network and the degree of complexity between the crack groups increase gradually. The overall fractal dimension of specimens 2#, 3#, and 4# is 2.017, 2.013, and 1.995, respectively, indicating that the overall fractal dimension of specimens shows a downward trend with the increase of discharge voltage, indicating that the crack openness increases and the roughness weakens. With the increase of smoothness, the main crack with a flat and flaky structure is more likely to appear, which can provide an unobstructed migration channel for coal-bed methane with an

ideal cracking effect. The numerical results of the fractal dimension are in good agreement with the fractal characteristics of the reconstructed three-dimensional cracks, and the crack distribution of the coal caused by high-pressure electric pulse water pressure conforms to the self-similar fractal distribution characteristics.

5. RESULT AND DISCUSSION

Coal-bed methane as a high quality civil and industrial power generator, automobile fuel, and important chemical raw material has important applications in many aspects. Although China has huge coal-bed methane reserves, limited by geological storage conditions and exploration technology, the utilization rate of coal-bed methane development in China is extremely low.

In this paper, the water shock wave waveform and parameters generated after high-voltage electric pulse discharge are measured by the water shock test system (Figure 5), and imported into PFC^{2D} to simulate the distribution and expansion law of cracks in coal rock under the action of high-voltage electric pulse hydraulic fracturing, which provides a basis for subsequent tests. The crack initiation and expansion law of coal rock under the action of 3 MPa water pressure and different discharge voltages was explored through the high-voltage electric pulse hydraulic cracking test platform (Figure 10). The crack area, volume damage factor, crack distribution angle, and fractal dimension of each crack were calculated and analyzed through CT scanning and three-dimensional reconstruction. With the hydrostatic pressure of 3 MPa unchanged, the number and distribution area of cracks (groups) in the coal core specimen gradually increase and become larger with the constant increase of discharge voltage, and the crack surface area, volume, complexity, and damage factor all show a steady increase trend. When the voltage changes from 11 kV to 13 kV, the crack damage area is increased by 2 times and the damage volume is increased by 10 times. The crack initiation mode, distribution area, number of statistical angles, and crack rate are closely related to angles. With the increase of discharge voltage, the crack initiation is concentrated from two symmetrical angles at first, and finally presents a 360-degree annular divergence distribution. The number of statistical angles decreases first and then increases, and finally forms a multiangle crack network. The crack distribution of coal induced by high-pressure electric pulse water pressure is consistent with self-similar fractal distribution characteristics. With the increase of discharge voltage, the fractal dimension of crack group increases, and the number of microcracks and the degree of bifurcation increase. The overall fractal dimension of the specimen decreases, the number of macroscopic cracks increases, the roughness between cracks decreases, and the smoothness increases, which can form an unobstructed coal-bed methane migration channel.

Based on the above research methods, the crack morphology and distribution law of coal rock under high voltage electric pulse hydraulic fracturing are studied visually and in three-dimensions from the mesoscopic perspective, which provides theoretical and experimental significance for the application of this technology in practical mining engineering in the future. Compared with traditional hydraulic fracturing, high voltage electric pulse hydraulic fracturing technology has the advantages of fast, cyclic loading, good fracturing effect, and a complex crack network, and can provide an unobstructed migration channel for coal-bed methane. However, in actual mining engineering, due to the influence of natural cracks and textures in coal rock, and the occurrence conditions of coal-bed methane, geological

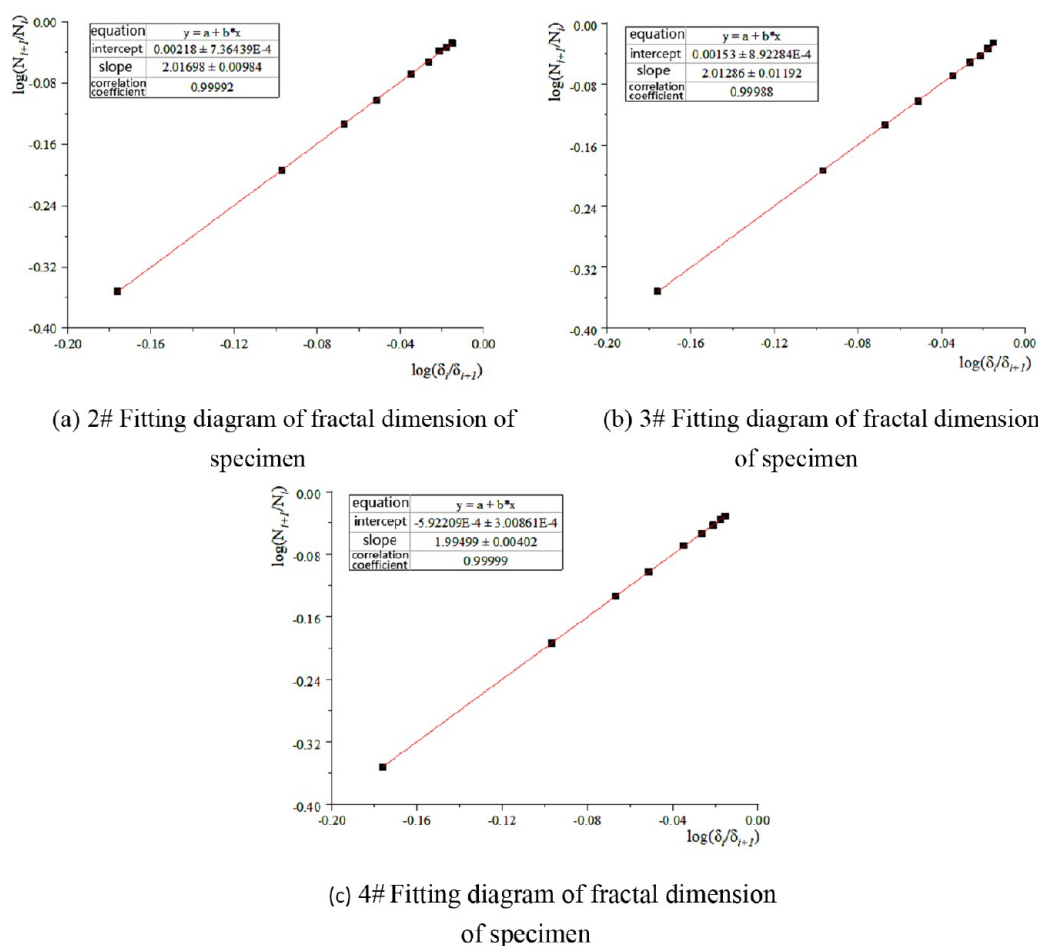


Figure 19. Fitting diagram of integral fractal dimension of each specimen.

movement, and groundwater, the application of this technology in engineering practice still needs a lot of theoretical and experimental support. In particular, the propagation law of a shock wave in different media, liquid–solid coupling relationship, fracture damage model, fracture damage constitutive relationship, and the efficient and accurate fracturing effect evaluation means need to be further discussed, which is also our next focus of research direction.

AUTHOR INFORMATION

Corresponding Author

Wu Zhang – School of Civil Engineering, Inner Mongolia University of Science and Technology, Baotou 014010, China; orcid.org/0000-0001-9151-9278; Email: Zhangwu2020023343@stu.imust.edu.cn

Authors

Xiankai Bao – School of Civil Engineering, Inner Mongolia Autonomous Region Building Structure Disaster Prevention and Mitigation Engineering Technology Research Center, and Inner Mongolia Autonomous Region Key Laboratory of Civil Engineering Safety and Durability, Inner Mongolia University of Science and Technology, Baotou 014010, China
 Shuang Zhao – School of Civil Engineering, Inner Mongolia University of Science and Technology, Baotou 014010, China
 Ning Wu – School of Civil Engineering, Inner Mongolia University of Science and Technology, Baotou 014010, China

Chaoyun Yu – School of Civil Engineering, Inner Mongolia University of Science and Technology, Baotou 014010, China
 Jinchang Zhao – School of Mining Engineering, Taiyuan University of Technology, Taiyuan 030024, China
 Wenxiang Zheng – School of Mining and Coal, Inner Mongolia University of Science and Technology, Baotou 014010, China

Complete contact information is available at: <https://pubs.acs.org/10.1021/acsomega.2c08178>

Notes

The authors declare no competing financial interest.

ACKNOWLEDGMENTS

The study was supported by Inner Mongolia Natural Science Foundation (grant no. 2020LH05018, grant no. 2019MS05053, grant no. 2020BS05017), Inner Mongolia University of Science and Technology Institute of Building Science Open Foundation (grant no. JYSJJ-2021M19, JYSJJ-2021Q06).

REFERENCES

- Zhai, C.; Wu, S.; Tang, Z.; Zhong, C.; Xu, J. Study on seam fracturing and permeability improved technology based on static blasting. *Coal Science and Technology*. **2015**, *43* (05), 54–57.
- Dong, Z.; Tang, S. Oriented perforation hydraulic fracture propagation based on the maximum tangential strain criterion. *Rock and Soil Mechanics*. **2019**, *40* (11), 4543–4553.

- (3) Hao, F.; Sun, L.; Liu, M. Research on boreholes space optimization of hydraulic flushing considering press relief and gas drainage effect. *Journal of Mining & Safety Engineering*. **2014**, *31* (5), 756–763.
- (4) Li, Y.; Bian, D.; Yan, D.; Xue, R. A coal seam anti-reflection experimental device based on high-voltage electric pulse. Shanxi: CN104061014A, 2014-09-24.
- (5) Bao, X. Mechanism and experimental study of high-voltage electric pulse hydraulic fracturing of coal. Thesis, Taiyuan University of Technology, Taiyuan. 2018.
- (6) Yutkin, S. *Hydraulic and Electric Effect*; Science Press: Beijing, 1962.
- (7) Buogo, S.; Cannelli, G. B. Implosion of an underwater spark-generated bubble and acoustic energy evaluation using the Rayleigh model. *Journal of the Acoustical Society of America*. **2002**, *111* (6), 2594–2600.
- (8) Timoshkin, I. V.; Fouracre, R. A.; Given, M. J.; MacGregor, S. J. Hydrodynamic modelling of transient cavities in fluids generated by high voltage spark discharges. *Journal of Physics D: Applied Physics*. **2006**, *39* (22), 4808–4817.
- (9) Rao, P.; Ouyang, P.; Nimbalkar, S.; Chen, Q.; Cui, J.; Wu, Z. Mechanism Analysis of Rock Failure Process under High-Voltage Electropulse: Analytical Solution and Simulation. *Materials*. **2022**, *15*, 2188.
- (10) Bao, X.; Guo, J.; Liu, Y.; Zhao, G.; Cao, J.; Wu, J.; Zhao, J. Damage characteristics and laws of micro-crack of underwater electric pulse fracturing coal-rock mass. *Theoretical and Applied Fracture Mechanics*. **2021**, *111* (5), 102853.
- (11) Jia, S.; Zhao, J.; Yin, Z.; Bian, D.; Yan, D.; Feng, J. Study on time variation of water shock front of coal based on high voltage electrical pulse reflection enhancement. *Journal of Taiyuan University of Technology*. **2015**, *46* (06), 680–684.
- (12) Li, C.; Zhao, Y.; Zhao, J.; Yang, S.; Ma, Z. Effect of prefabricated cracks on High voltage electric pulse fracturing coal and rock mass in water. *Coal Mine Safety*. **2021**, *52* (07), 27–32.
- (13) Bao, X.; Liu, Y.; Guo, J.; Chao, J.; Zhao, J.; Wu, J. Quantitative evaluation of fracturing effect of coal-rock masses under high-voltage discharge actions in water. *Chinese Journal of Rock Mechanics and Engineering*. **2019**, *39* (04), 715–725.
- (14) Zhiqiang, Y.; Jinchang, Z.; Decun, B.; Dong, Y.; Shaohua, J. I. A. Study on delay and current characteristics of High voltage pulse Discharge in water [J]. *Journal of Taiyuan University of Technology* **2016**, *47* (03), 326.
- (15) Bao, X.; Duan, D.; Cao, J.; Wu, J.; Zhao, J. Study on the effect and law of electric pulse hydraulic fracturing in low permeability coals. *Oil and Gas Reservoir Evaluation and Development*. **2018**, *8* (05), 64–69.
- (16) Bao, X.; Cao, J.; Zheng, W.; Guo, J.; Liu, Y.; Zhao, J. Study on the Damage Model of Coal Rock Caused by Hydraulic Pressure and Electrical Impulse in Borehole. *Geofluids*. **2021**, *2021* (3), 1–19.
- (17) Bao, X. K.; Cao, J. X.; Duan, D. M.; Zhao, J. C.; Wu, J. W. Mechanism and numerical simulation of CBM extraction by pulsed discharge fracturing in water. *Petroleum Reservoir Evaluation and Development*. **2019**, *9* (02), 71–74.
- (18) Zhang, J. *Development of rock meso-damage visualization system and study on the evolution of pore and fissure structure*. Taiyuan University of Technology, Taiyuan, 2019.
- (19) Zhao, J.; Feng, Z.; Yang, D.; Kang, Z. Study of pyrolysis of oil shale based on 3D CT images. *Chinese Journal of Rock Mechanics and Engineering*. **2014**, *33* (1), 112–117.
- (20) Li, Y.; Zhang, Y.; Cong, L.; Xie, Z.; Yan, M.; Tian, X. Application of X-CT scanning Technique in the Characterization of Micro pore structure of Tight sandstone Reservoir: An Example from Fuyu oil layer in Daan oil field. *Journal of Jilin University (Earth science Edition)*. **2016**, *46* (2), 379–387.
- (21) Wang, Y.; Wang, L. H.; Wang, J. Q.; Jiang, Z.; Jing, C.; Wang, Y. F. Investigation of organic matter pore structures of shale in three dimensions of shale using nano-X-ray microscopy. *Rock and Mineral Analysis*. **2017**, *36* (6), 563–573.
- (22) Fu, Y.; Chen, X.; Feng, Z. Characteristics of coal-rock fractures based on CT scanning and its influence on failure modes. *Journal of China Coal Society*. **2020**, *45* (2), 568–578.
- (23) Wang, G.; Yang, X.; Zhang, X.; Li, W.; Shi, L. Numerical simulation of gas seepage in pore sand fissures of coal rock mass based on the DTM threshold segmentation method. *Chinese Journal of Rock Mechanics and Engineering*. **2016**, *35* (1), 119–129.
- (24) Guofang, L. I. U.; Xuanmin, S.; Yuming, H. U. O. Micro-structure numerical reconstruction of fractured coal body based on CT technology. *Mining Research and Development*. **2020**, *40* (8), 155–159.
- (25) Yunhe, B. *Analysis of the variation law of segmental fracturing stress field in volcanic rock horizontal wells*; Northeast Petroleum University.: Daqing, 2019. DOI: 10.26995/d.cnki.gdqsc.2019.000050.
- (26) Liu, X.; Dai, F.; Liu, J.; Zhang, Ru. Experimental study on static and dynamic Brazilian splitting of coal rocks considering laminar orientation. *Journal of Rock Mechanics and Engineering*. **2015**, *34* (10), 2098–2105.
- (27) Liu, S.; Cui, Y.; Cui, S.; Li, Z.; Zhou, F.; Wang, H. Experimental investigation on rock fracturing performance under high-pressure foam impact. *Engineering Fracture Mechanics*. **2021**, *252*, 107838.
- (28) Cao, C.; Hua, J. *Engineering fracture mechanics*; Xi'an Jiaotong University Press, 2015.
- (29) Zhou, T.; Yang, X.; Han, X. Numerical inversion simulation of coal rock under uniaxial compression failure in PFC2D. *Journal of mining science and technology*. **2017**, *2* (03), 260.
- (30) GB/T 50266-2013, *Standard for engineering rock mass test methods*; Chinese National Standard, MOHURD, 2013.
- (31) Cao, J. Study on the macro- and meso-damage behavior and law of high-voltage pulse hydraulic fracturing rock mass. *Inner Mongolia University of Science and Technology*. **2020**, DOI: 10.27724/d.cnki.gnmkg.2020.000393.
- (32) Guo, H.; Wang, K.; Cui, H.; Xu, C.; Yang, T.; Zhang, Y.; Teng, T. Experiment investigation on the pore and fracture structure of the reconstructed coal and its fractal characteristic. *Journal of China university of mining and technology*. **2019**, *48* (06), 1206–1214.
- (33) Sun, B. The Fractal dimension and its measurement methods. *Journal of northeast forestry university*. **2004**, *16* (03), 116–119.